J Mater Sci: Mater Electron
DOI 10.1007/s10854-016-6168-8

Mechanical properties enhancement in potassium-sodium niobate lead-free piezoceramics: the impact of chemical modifications

L. Ramajo[1] · M. Castro[1] · J. F. Fernandez[2] · F. Rubio-Marcos[2]

Received: 22 August 2016 / Accepted: 29 November 2016

Abstract The development of $(K_{0.44}Na_{0.52}Li_{0.04})(Nb_{0.86}Ta_{0.10}Sb_{0.04})O_3$-based (KNL-NTS) ceramics is attracting great interest because of environmental concerns. Most of the efforts have been concentrated on improving the electrical properties. However, it is desirable to develop ceramics with good electrical response and high mechanical properties. Therefore, the evaluation of the mechanical properties is substantial and little studied. The aim of this work is to study the mechanical properties of KNL-NTS lead free ceramics doped with Zr evaluating the effects that can give rise to improved mechanical properties. Our results show that the crystalline phase, size and shape of grains in the ceramics are affected by the doping amount. We found that the microstructure does have a close relationship to the mechanical response, more specifically; a uniform and fine grain microstructure is suitable to lead high mechanical strength. Based on these results, the chemical modifications with Zr^{4+} ions have a significantly positive influence on hardness, strength and fracture toughness values of KNL-NTS ceramics.

1 Introduction

Legal restrictions on the use of lead in electric and electronic devices have been increasing the efforts related to the development of lead-free alternatives to lead zirconate titanate (PZT)-based piezoelectric ceramics [1, 2]. Recent reports have indentified many possible lead-free candidates based on potassium sodium niobate $(K,Na)NbO_3$ (KNN); $(Na,Bi)TiO_3$ (NBT) and $(K,Bi)TiO_3$ (KBT) [3–6].

The KNN phase was discovered in the late 1950s, with a piezoelectric coefficient (d_{33}) of about 80 pC/N, a Curie temperature of 420 ºC,and a formulation close to the morphotropic phase boundary (MPB) [4]. Nevertheless, it is difficult to obtain pure KNN-based ceramics with high density and great piezoelectric performance. Saito et al. made a break-through in the system $(K,Na)NbO_3$–$LiTaO_3$–$LiSbO_3$ (KNL-NTS), reporting exceptionally high piezoelectric properties [7]. This pioneering study was based on chemical modifications, in the vicinity of the MPB of $(K,Na)NbO_3$ (KNN), by complex simultaneous substitutions in the A (Li) and B (Ta and Sb) site of the perovskite lattice. Besides these chemical modifications, they developed a novel processing route for producing textured polycrystals of the KNN-based compositions by additional engineering of the microstructural design [7, 8].The potassium–sodium niobate system is of particular interest due to its large electrical properties. However, it is highly desirable to develop KNN-based materials possessing both a large electrical response and high mechanical properties. Therefore, the characterization of the mechanical properties of this material is an important subject, and still little studied in the literature.

With regards to the mechanical properties like toughness and stiffness in piezoelectric ceramics, they depend on many factors, such as microstructure composition and

L. Ramajo and F. Rubio-Marcos have contributed equally.

✉ L. Ramajo
lramajo@fi.mdp.edu.ar

[1] Institute of Research in Materials Science and Technology (INTEMA), Juan B. Justo 4302 (B7608FDQ), Mar del Plata, Argentina

[2] Electroceramic Department, Instituto de Cerámica y Vidrio, CSIC, Kelsen 5, 28049 Madrid, Spain

crystallographic phases, polarization state, loading type and direction, loading rate and electrical boundary conditions [9]. Commercial piezoelectric PZT-based ceramics show low fracture toughness (~1.0 MPa.m$^{1/2}$), which makes them susceptible to fracture [10]. Whereas, research related to fracture behavior of these ceramics is therefore of considerable importance by increase the lifetime of piezoelectric devices, especially for actuators devices. Defects are present in ceramics, raising the stress concentrations under high electrical fields and/or mechanical stresses leading to crack growth which may result in the degradation of the electromechanical properties or device failure. Consequently, it is necessary to examine the fracture resistance of lead-free ceramics which can possibly replace or improved of PZT based ceramics.

In recent publications the fracture toughness of KNN-based ceramics was investigated using indentation fracture methods. Andrejovská et al. [11] and Zhang et al. [12] obtained fracture toughness in pure KNN and doped KNN close to 1.0 ± 0.1 MPa.m$^{1/2}$ and 1.5 ± 0.2 MPa.m$^{1/2}$, respectively.

The aim of this communication is to study the mechanical properties of $(K_{0.44}Na_{0.52}Li_{0.04})[(Nb_{0.86-x}Ta_{0.10-x}Sb_{0.04-x})Zr_{5x/4}]O_3$ lead-free ceramics (KNL−$(NTS)_{1-x}Zr_{5x/4}$) and to address effects that can give rise to mechanical properties enhancement. Therefore, in order to introduce the Zr^{4+} ion into the B-site of the perovskite lattice, we selected the B-site deficiency, with a global formula $(K_{0.44}Na_{0.52}Li_{0.04})[(Nb_{0.86}Ta_{0.10}Sb_{0.04})_{1-x}Zr_{5x/4}]O_3$.To reach this objective, we show that the chemical modifications by replacement of the B-sites with Zr^{4+} ions on (K,Na)NbO_3-based materials produces a high impact on the crystal structure, and the microstructure of the ceramics. As a consequence, we found that the mechanical properties present a clear relationship with the final microstructure of the system, which is governed by the introduction of the Zr^{4+} ions and their increased content.

2 Experimental procedure

2.1 Preparation process

The $(K_{0.44}Na_{0.52}Li_{0.04})[(Nb_{0.86}Ta_{0.10}Sb_{0.04})_{1-x}Zr_{5x/4}]O_3$ composition was prepared by the conventional ceramic processing route. Na_2CO_3, Li_2CO_3 (Panreac, 99.5%), K_2CO_3 (Merck, 99%), ZrO_2, Nb_2O_5, Ta_2O_5, and Sb_2O_5 (Sigma–Aldrich, ≥ 99.5%, 99.9%, 99% and 99.995%, respectively) were used as starting raw materials. They were individually milled in order to obtain an appropriate distribution of the particle size.

Powders with different ZrO_2 concentrations (x = 0.00, 0.005, 0.01, 0.03 and 0.05), abbreviated as KNL−$(NTS)_{1-x}Zr_{5x/4}$, were weighted by electronic balance and ball milled for 3 h in ethanol medium in a high energy laboratory ball-mill with zirconia balls. Afterwards, the resulting powders were dried and calcined at 700 °C for 2 h at 3 ºC/min. The calcined powders were attrition milled again and pressed at 200 MPa into disks of 10 mm in diameter and 0.7 mm thick. The pellets were finally sintered in air at 1125 ºC for 2 h. The sintered temperature was selected taking into account previous studies of the authors [13].

2.2 X-ray diffraction (XRD)

Crystalline phases were characterized by X-ray diffraction (XRD) (D8 Advance, Bruker, Germany), using CuK_α radiation, on powders obtained by milling the sintered ceramics.

2.3 Microstructural characterization

Microstructure was evaluated on polished and thermally etched samples (1000 °C for 5 min) using a Field Emission Scanning Electron Microscope, FE-SEM (Hitachi S-4700). Grain size distributions (GSD) and the average grain size (AGS) were measured from the FE-SEM micrographs using an image analysis program (Leica Qwin, Leica Microsystems Ltd, Cambridge, England) considering more than 300 grains in each measurement.

2.4 Mechanical characterization:

Elastic modulus and hardness were measured by means of a HysitronTriboindenter. A Berkovich diamond indenter with a total included angle of 142.3° was used for every measurement of 25 load–unload cycles with 5000 μN. The data sets were processed using an appropriate software to produce load–displacement curves [14].

The Oliver–Pharr method [15], which proposes the estimation of the slope of the unloading curve by first fitting the entire unloading data, was employed to determine the reduced elastic modulus (E_r) and the hardness (H) of the materials. The reduced elastic modulus is related to the elastic modulus of the sample (E) and the contact stiffness (S) by Eqs. (1) and (2):

$$1/E_r = (1 - \nu^2)/E + (1 - \nu_i^2)/E_i \quad (1)$$

$$E_r = S(\pi/4A_{max})^{1/2} \quad (2)$$

where υ is the Poisson's ratio and subscript i denotes the indenter material. A_{max} is the surface contact area at the maximum displacement. The contact stiffness (S) is the slope of the unloading curve taken as the first derivative in the maximum depth of a fitted power law function of the unloading segment of the curve. For our indenter

tip, E_i is 1140 GPa and υ_i is 0.07, while ceramics Poisson's ratio was assumed to be 0.25.

The material hardness (H) was defined as the maximum load, P_{max}, divided by the projected area of the indentation under this load, Eq. (3):

$$H = P_{max}/A_{max}. \quad (3)$$

The tip area function $A(hc)$ was calibrated from indentations upon a fused silica sample of known E.

The K_{IC} values were determined using the direct crack measurement method. Vickers indentations method (Fig. 1) and the cracks originated from Vickers indentations were used to obtain the Vickers´s hardness and toughness by Anstis method [16]. Toughness measured by Anstis crack-length method is dependent on the elastic modulus of the material, microindentation, hardness and crack length, and the applied load [17, 18]. It employed a simplified two-dimensional fracture mechanics and obtained:

$$K_{IC} = 0.016 \times (E/H)^{1/2} \times F/c^{3/2} \quad (4)$$

where F is the lo ad in Newton, c is the crack length from the center of the indent to the crack tip in meters, E is the Young's modulus in GPa and H is the Vickers hardness in GPa.

2.5 Electrical characterization

For the electrical measurements, silver pastes were coated on both sides of the sintered samples. After firing at 600 °C for 30 min, these samples were used for characterizing electrical performance. In order to test the piezoelectric constant, the samples were polarized under a direct current (dc) electric field of 4 kV/mm in a silicone oil bath at 25 °C for 30 min. The piezoelectric constant $d_{33}$was measured using a piezo d_{33} meter (YE2730A d_{33} METER, APC International, Ltd., USA) at room temperature.

3 Results and discussion

A classical technique to seek structure information on lead-based piezoceramics is X-ray diffraction. Figure 2 presents the X-ray diffraction patterns of KNL−$(NTS)_{1-x}Zr_{5x/4}$ ceramics for different ZrO_2 amounts and sintered at 1125 °C for 2 h. All main diffraction patterns correspond to a perovskite structure. Although, the presence of a minor secondary phase was detected in undoped samples, typical secondary impurity phases were not observed in doped-samples. In particular, the absence of secondary impurity phases in doped samples, which are assigned to $K_6LiNb_6O_{17}$ (PDF# 36-0533) or $K_6Nb_{10.88}O_{30}$ (PDF# 87-1856) with tungsten-bronze type (TTB) [19, 20], is a

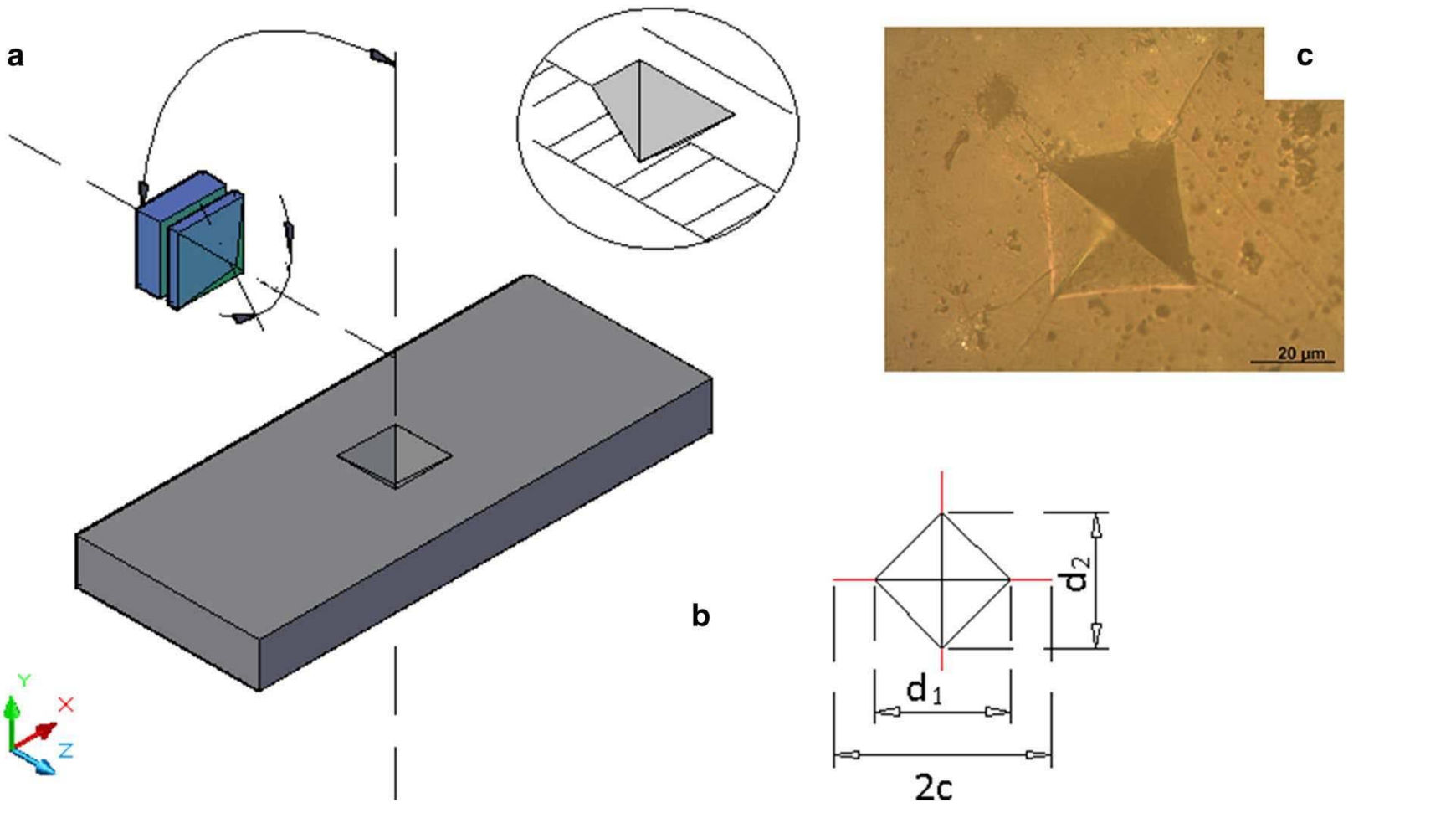

Fig. 1 Vickers hardness testing. **a** Schematic of a Vickers or diamond pyramid hardness indenter. The indentation depth h is approximately 1/7 of the average length D of the diagonal [17]. **b** Schema of a Vickers indentation. **c** Vickers indentation on a radial cross section of KNL-NTS ceramics. The load on the indenter was 5 N, and the dwell time was 10 s

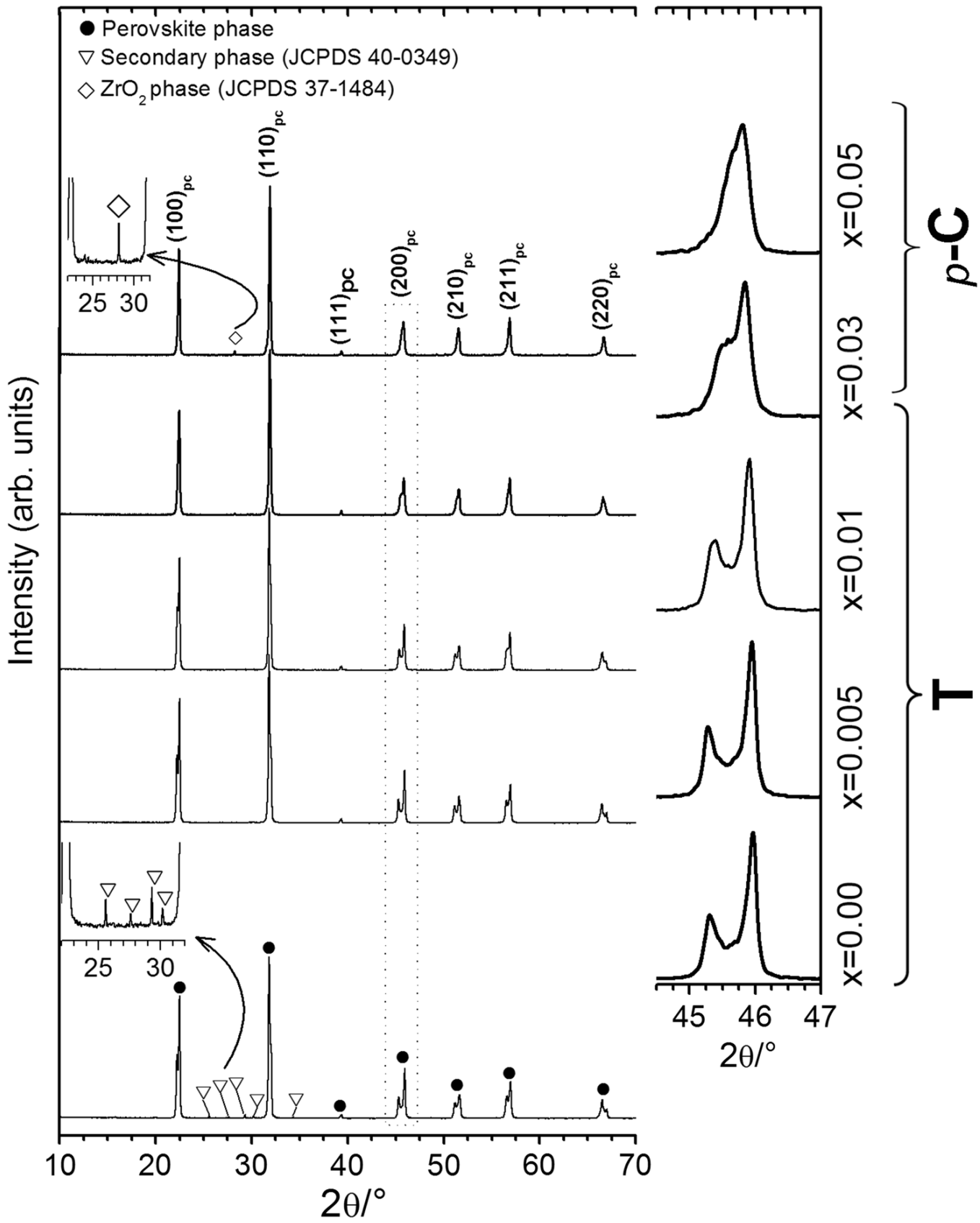

Fig. 2 Influence of the ZrO_2 concentration in the crystalline structure of the $KNL-(NTS)_{1-x}Zr_{5x/4}$ ceramic system: the figure shows X-ray diffraction patterns of $KNL-(NTS)_{1-x}Zr_{5x/4}$ ceramics sintered at 1125 °C for 2 h. In samples with high ZrO_2 content ($x > 0.03$) appears a different peak associated with unreacted ZrO_2 particles. The *insets* of each figure show a detail of the XRD diffraction pattern in the 2θ range 44.5° to 47° of the $KNL-(NTS)_{1-x}Zr_{5x/4}$ ceramics. On the right, crystal symmetry evolution of the perovskite structure induced by the Zr^{4+} doping.(*T* tetragonal symmetry, and *p-C pseudo*-cubic symmetry)

remarkable result because these TTBs phases are commonly present in sintered alkaline niobates and form liquid phases that affect piezoelectric response [21]. However, we can also detect that there is a different trend for the ceramic with the higher Zr^{4+} content ($x \geq 0.05$). In this composition, $x \geq 0.05$, the XRD pattern shows peaks associated with the presence of unreacted ZrO_2 particles (JCPDS# 37-1484), showing that the Zr^{4+} cannot be incorporated into the KNL-NTS structure.

Moreover, as represented in the insets of the Fig. 2, the Zr^{+4} doping produces a high impact on the perovskite structure. The insets show a detail of the XRD diffraction pattern in the 2θ range 44.5° to 47° of the $KNL-(NTS)_{1-x}Zr_{5x/4}$ ceramic system as a function of the Zr^{4+} content. From the insert, we can infer that the Zr^{4+} doping induces a phase diffusion transition between a main Tetragonal phase (**T**) to an apparently *pseudo*-Cubic phase (***p*-C**). Therefore, the most probable origin of this behavior must be related to the solubility of Zr^{4+} ions into the perovskite structure. Therefore, we suppose that the gradual entry of Zr^{4+} ions into the $KNL-(NTS)_{1-x}Zr_{5x/4}$ perovskite lattice produces an evolution in the crystal symmetry suppressing the ***T*** phase in favor of *p*-***C*** phase.

Considering the XRD results, two aspects can be highlights; first, for a low doping range, the apparition of TTBs impurity phases is inhibited; and secondly, for a high doping range, the ***T*** phase is suppressed in favour of a new ***p*-C** phase transition. Furthermore, in this last case, the solubility of Zr^{4+} ions in the perovskite structure is exceeded, provoking the apparition of an unreacted ZrO_2 phase.

As previously mentioned in the see Sect. 1, the microstructural features play a relevant role on the mechanical properties of the piezoceramics and, therefore, their morphology and distribution can be used to plan new strategies in designing new materials with improved mechanical properties. Figure 3 shows the changes generate on the microstructure and the grain size distribution (GSD) of the ceramics by adding Zr^{4+} ions. Figure 3a–e shows a sequential FE-SEM images of the chemical etched surface of the KNL−$(NTS)_{1-x}Zr_{5x/4}$ ceramics for different Zr^{4+}contents. These micrographs indicated that Zr doping causes a significant change in the grain shape and size. The average grain size (AGS) of KNL−$(NTS)_{1-x}Zr_{5x/4}$ ceramics increases with growing Zr^{4+} content ($x \leq 0.005$, Fig. 3a, b) and then drops dramatically with further increasing Zr^{4+} content ($0.01 \leq x \leq 0.05$, Fig. 3c–e). These two dissimilar performances could be firstly attributed to the formation of a liquid phase during the sintering process for low Zr contents ($0.00 \leq x \leq 0.005$) [22, 23]. According to the phase diagram, the niobium excess forms a liquid phase at ~1058 °C that could promote sintering with grain coarsening [21]. Hence, the addition of acceptor dopants increase de diffusivity and promotes the grain growth, increasing the grain size [23, 24]. And secondly, for high Zr contents ($0.01 \leq x \leq 0.05$), the Zr^{4+} ions should acts as a grain growth inhibitor, and additionally transforms the grain shape into more cube-shaped grains with sharp edges and corners. Figure 3f-j plots the GSDs of KNL−$(NTS)_{1-x}Zr_{5x/4}$ ceramics for different Zr content. Comparing the GSDs evolution, two remarkable observations can be made again. Firstly, the ceramics with $0.00 \leq x \leq 0.005$ have multimodal distribution of grain sizes, that is, bigger grains are surrounded by smaller ones, and secondly, increasing the Zr^{4+} content the GSDs evolves toward a unimodal distribution.Thus, one can consider that the system evolves to a more homogeneous grain size distribution. In addition, from the GSDs, it can also be observed that the average grain size (AGS) decrease from $\sim 1.98 \pm 1.2$ μm in the undoped ceramic ($x = 0.00$), to sub-micrometer size of $\sim 0.63 \pm 0.40$ μm for the ceramics with the highest Zr^{4+} content ($x \geq 0.05$). As a result, the mass transportation during sintering is weakened and grain growth is inhibited which is similar to other reports on different systems [24, 25]. In addition, at high concentrations of Zr^{4+} ions, unreacted ZrO_2 phase is detected by XRD (as evidenced in Fig. 2). This phase can be concentrated and/or segregated close to the grain boundaries and thus decreases the mobility of the grain boundary. This also acts as an inhibitor of grain growth. Thus, our results show that the size and shape of grains in the ceramics are strongly affected by the doping amount of Zr^{4+} ions.

The measured density (ρ), piezoelectric constant (d_{33}), average grain size (D_{50}), hardness (H_v), fracture toughness (K_{IC}) and elastic modulus (E) of KNL−$(NTS)_{1-x}Zr_{5x/4}$ ceramics with x between 0.00 and 0.05 are shown in Table 1. It can be seen that, at low zirconium concentrations, piezoelectric constant d_{33} increases with Zr addition, while d_{33} decreases at higher Zr amounts. This behavior was also observed in other KNL-NTS systems [20]. For mechanical properties, similar values to those reported by Yilmaz et al. [9] for analogous KNN systems and by Bermejo et al. [24] in PZT systems are shown. However, in this case it can be observed that the lower values of the

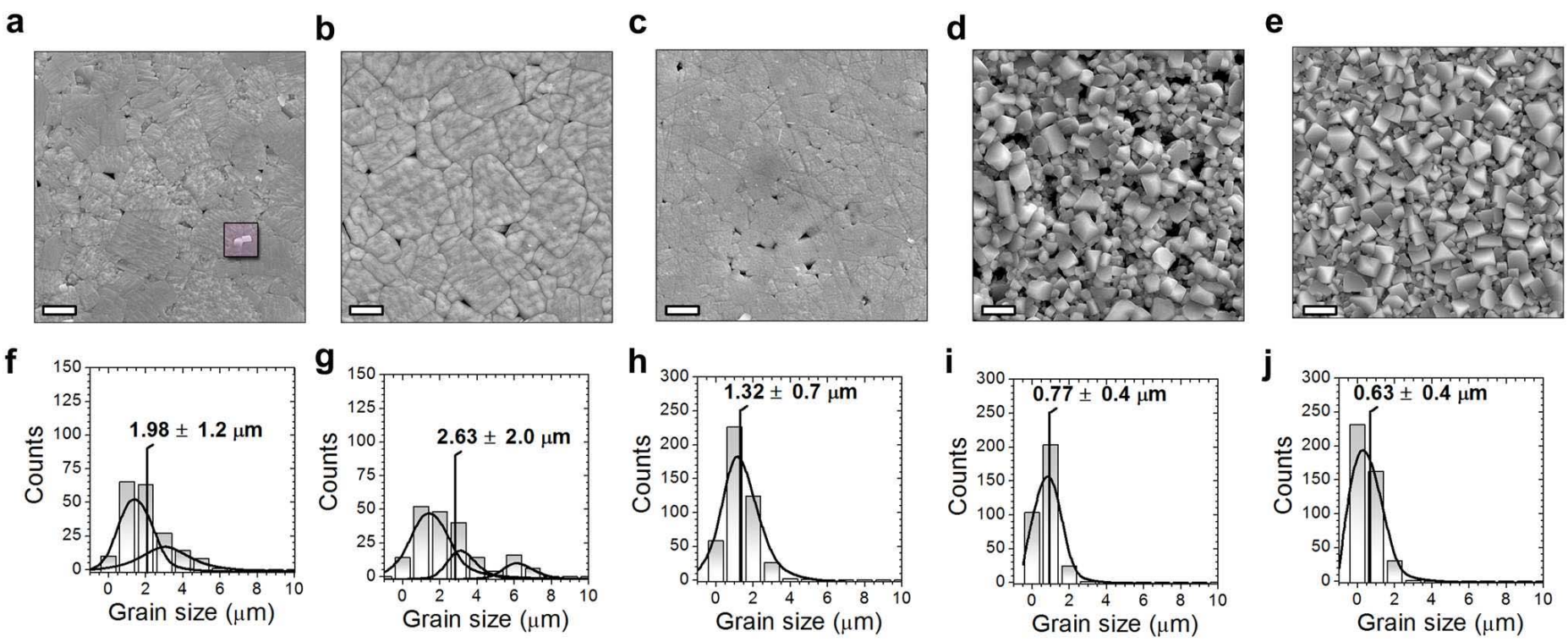

Fig. 3 **a–e** Sequence of FE-SEM images showing the evolution of the microstructure in the KNL−$(NTS)_{1-x}Zr_{5x/4}$ for different contents of Zr^{4+}, corresponding **a** to undoped, **b** to $x = 0.005$, **c** to $x = 0.01$, **d** to $x = 0.03$, and **e** to $x = 0.05$. The *marked square* in the *panel***a** shows the location of secondary impurity phase assigned to TTB phase, which was previously detected by XRD. *Scale bar*, 2 μm. On bottom, (**f–j**) Sequence of particle size distributions (PSD) for each composition

Table 1 Relative density, piezoelectric constant, average grain size, fracture toughness, elastic modulus and harness obtained by nanoindentation of the KNL−(NTS)1−xZr5x/4 samples sintered at 1125 °C for 2h with 0 to 0.05 mol.% of Zr

KNL−$(NTS)_{1-x}Zr_{5x/4}(x)$	ρ(g/cm^3)	d_{33} pC/N	D_{50} (μm)	K_{IC}[a] (MPa.m$^{1/2}$)	E (GPa)	H (GPa)
0.000	4.42 ± 0.13	205	1.98 ± 1.2	0.65 ± 0.087	101.9 ± 18.1	6.4 ± 1.8
0.005	4.43 ± 0.07	270	2.64 ± 2.0	0.79 ± 0.089	136.2 ± 6.9	9.4 ± 0 0.7
0.010	4.40 ± 0.09	210	1.32 ± 0.7	0.84 ± 0.072	129.5 ± 7.5	9.2 ± 1.3
0.030	4.60 ± 0.04	115	0.77 ± 0.4	0.81 ± 0.051	133.4 ± 9.2	9.6 ± 1.4
0.050	4.58 ± 0.03	70	0.63 ± 0.4	1.08 ± 0.107	128.9 ± 10.1	9.7 ± 0.7

[a] $K_{IC} = 0.016(E/H)^{1/2}xF/c^{3/2}$

hardness and fracture toughness are revealed in undoped KNL-NTS ceramic according to the highest grained structure and porosity.By increasing the amount of the Zr^{4+} ions into KNL-NTS perovskite structure, the values of the mechanical properties such as hardness, fracture toughness and elastic modulus are also increased. The hardness value of the pure KNL-NTS ceramic increased from approximately 6.4 to 9.7 GPa when 0.05% of Zr was added into the ceramic, while the fracture toughness increased from 0.65 to approximately 1.08 MPa.m$^{1/2}$ when 0.05% of Zr was added.

There are main factors that can explain this change on the mechanical properties due to the Zr^{4+} concentration effects. First, the phase coexistence between two or more phases in some samples contributes to the fracture toughness values since phase coexistence multiplies the number of possible polarization directions in the samples, which facilitate the domain motion under an external electric field or mechanical stress [26]. Some researchers report that domain wall motion also contributes to the fracture toughness of ferroelectric ceramics by energy dissipation [27–30]. This justification cannot completely explain the obtained results because, in this case, ZrO_2 addition in higher concentration induces a phase diffusion transition between a main ***T*** phase to *p*-***C*** phase. Second, it has been known that the addition of solutes atoms can harden some materials, and then it is possible that in this case the variation of ionic size in the lattice could moderately inhibit the deformation caused by the hardness indenter and resulted in an increase in hardness and elastic modulus with the increasing Zr content [32]. Similarly, Watcharapasorn et al. reported an improvement on mechanical properties in zirconium-doped bismuth sodium titanate ceramics attributed to this phenomenon [33]. In this work, we found that the phase structure is not the only factor related to mechanical properties of the system. Hence,from a microstructural perspective, as indicated in Table 1, there is a growing trend for mechanical values with the introduction of the Zr^{4+} ions and their increased content. As a result, the microstructure has a close relationship to the mechanical properties, that is, a uniform and fine grain microstructure is suitable to lead highmechanical strength.

4 Conclusions

$(K_{0.44}Na_{0.52}Li_{0.04})(Nb_{0.86-x}Ta_{0.10-x}Sb_{0.04-x})Zr_{5x/4}O_3$ ceramics were successfully prepared by a solid-state mixed-oxide method. Microstructure, and mechanical properties of the ceramics were affected by the addition of ZrO_2. The implication derived from this study is that we can surprisingly modulate the final microstructure of the KNL−$(NTS)_{1-x}Zr_{5x/4}$ lead–free system by the replacement of the B-sites with Zr ions in the perovskite structure. Therefore, we have stabilized a microstructure with a uniform and sub-micrometer grain size, which is suitable as it lead to mechanical properties enhancement of this system. The results presented here reveal that the control of ceramic microstructure is regulated by the introduction of the Zr^{4+} ions and the doping amount. Consequently, the chemical modifications with Zr^{4+} ions have a significantly positive influence on mechanical properties of KNL-NTS lead–free ceramics, obtaining values comparable to PZT ceramics.

Acknowledgements The authors are grateful to CONICET, ANPCyT, University of Mar del Plata (Argentina) and to MICINN (project MAT 2010-21088-C03-01) for the financial support provided for this research. Dr. F. Rubio-Marcos is also indebted to the MINECO (Spain) project MAT2013-48009-C4-1-P for their financial support. Dr. F. Rubio-Marcos is also indebted to MINECO for a ‘‘Juan de la Cierva’’ contract (ref: JCI-2012-14521), which is co-financed with European Social Fund.

Compliance with ethical standards

Conflict of interest The authors declare no conflict of interests.

References

1. Z.P. Yang, Y.F. Chang, H. Li, Piezoelectric and dielectric properties of PZT–PZN–PMS ceramics prepared by molten salt synthesis method. Mater. Res. Bull. **40**, 2110–2119 (2005)
2. H. Du, S. Qu, J. Che, Z. Liu, X. Wei, Z. Pei, The effect of composition on microstructure and properties of PNW–PMS–PZT ceramics for high-power piezoelectric transformer. Mater. Sci. Eng. A **393**, 36–41 (2005)

3. L. Ramajo, M. Castro, F. Rubio-Marcos, J. Fernandez-Lozano, Influence of MoO_3 on electrical and microstructural properties of $(K_{0.44}Na_{0.52}Li_{0.04})(Nb_{0.86}Ta_{0.10}Sb_{0.04})O_3$. J. Mater. Sci.: Mater. Electron. **24**(9), 3587–3593 (2013)
4. K. Wang, J. Li, N.F. Liu, Piezoelectric properties of low-temperature sintered Li-modified (Na, K)NbO_3 lead-free ceramics. Appl. Phys. Lett. **93**, 092904 (2008)
5. J. Camargo, L.A. Ramajo, F. Rubio-Marcos, M. Castro, Ferroelectric Properties of $Bi_{0.5}(Na_{0.8}K_{0.2})_{0.5}TiO_3$ Ceramics. Adv. Mater. Res. **975**, 3–8 (2014)
6. A. Thongtha, T. Bongkarn, Optimum Sintering Temperature for Fabrication of $0.8Bi_{0.5}Na_{0.5}TiO_3$-$0.2Bi_{0.5}K_{0.5}TiO_3$ Lead-Free Ceramics by Combustion Technique. Key Eng. Mater. **474**, 1754–1759 (2011)
7. Y. Saito, H. Takao, T. Tani, T. Nonoyama, K. Takatori, T. Homma, T. Nagaya, M. Nakamura, Lead-free piezoceramics. Nature **432**, 84–87 (2004)
8. F. Rubio-Marcos, J.J. Romero, M.S. Martín-Gonzalez, J.F. Fernández, Effect of stoichiometry and milling processes in the synthesis and the piezoelectric properties of modified KNN nanoparticles by solid state reaction. J. Eur. Ceram. Soc. **30**, 2763–2771 (2010)
9. E.D. Yilmaz, H.E. Mgbemere, H. Özcoban, R.P. Fernandes, Investigation of fracture toughness of modified $(K_xNa_{1-x})NbO_3$ lead-free piezoelectric ceramics, J. Eur. Ceram. Soc. **32**, 3339–3344 (2012)
10. G.A. Schneider, Influence of electric field and mechanical stresses on the fracture of ferroelectrics. Ann. Rev. Mater. Res. **37**, 491–538 (2007)
11. J. Andrejovská, J. Mihalik, V. Kova, H. Bruncková, DuszaJ, Microstructure and fracture-mechanical properties of Pb free piezoelectric ceramics on the base $(Na_{0.5}K_{0.5})NbO_3$. Powder Metall. Prog. **9**, 228–231 (2009)
12. H. Zhang, S. Yang, S. Yang, D. Kong, B-P. Zhang, Y. Zhang, Reliability enhancement in nickel-particle-dispersed alkaline niobate piezoelectric composites and actuators. J. Eur. Ceram. Soc. **31**, 795–800 (2011).
13. Rubio-Marcos, (2010), PhDThesis, Instituto de Cerámica y Vidrio, Madrid, Spain
14. M.A. Ramírez, R. Parra, M.M. Reboredo, J.A. Varela, M.S. Castro, L. Ramajo, Elastic modulus and hardness of $CaTiO_3$, $CaCu_3Ti_4O_{12}$ and $CaTiO_3/CaCu_3Ti_4O_{12}$ mixture, Mater. Lett. **31**, 1226–1228 (2010)
15. W.C. Oliver, G.M. Pharr, Improved technique for determining hardness and elastic modulus using load and displacement sensing indentation experiments, J. Mater. Res. 7,1564–1580 (1992)
16. K. Strecker, S. Ribeiro, M.J. Hoffmann, Fracture toughness measurements of LPS-SiC: a comparison of the indentation technique and the SEVNB method, J. Mat. Res. **8**, 121–124 (2005)
17. O. Sahin, O. Uzun, U. Kolemen, N. Ucar, Vickers microindentation hardness studies of β-Sn single crystals, Mater. Charact. **58**, 197–204 (2007)
18. M. Majić, L. Ćurković, D. Ćorić, Load dependence of the apparent Knoop hardness of SiC ceramics in a wide range of loads, Materialwiss. Werkstofftech. **42**, 234–238 (2011)
19. L.A. Ramajo, J. Taub, M.S Castro, Effect of ZnO addition on the structure, microstructure and dielectric and piezoelectric properties of $K_{0.5}Na_{0.5}NbO_3$ Ceramics. Mater. Res. **17**, 728–733 (2014)
20. L. Ramajo, M. Castro, A. del Campo, J.F. Fernandez, F. Rubio-Marcos, Revealing the Role of Cationic Displacement in Potassium-Sodium Niobate Lead-free Piezoceramics by adding W^{6+} ions. J. Mater. Chem. C **3**, 4168–4178 (2015)
21. F. Rubio-Marcos, P. Ochoa, J. Fernandez, Sintering and properties of lead-free (K, Na,Li)(Nb,Ta,Sb)O_3 ceramics. J. Eur. Ceram. Soc. **27**, 4125–4129 (2007)
22. J. Wang, X. Chen, X. Zhao, X. Liang, X. Liu, P. Liu, Structure and dielectric property of Zr-doped $(Na_{0.47}Bi_{0.46}Ba_{0.06}K_{0.01})(Nb_{0.02}Ti_{0.98})O_3$ lead-free ceramics. J. Electroceram. **32**, 332–338 (2014)
23. X. Wang, J. Wu, X. Cheng, B. Zhang, J. Zhu, D. Xiao, Compositional dependence of phase structure and electrical properties in $(K_{0.50}Na_{0.50})_{0.97}Bi_{0.01}(Nb_{1-x}Zr_x)O_3$ lead-free ceramics. Ceram. Int. **39**, 8021–8024 (2013)
24. X. Vendrell, J.E. García, X. Bril, D.A. Ochoa, L. Mestres, G. Dezanneau, Improving the functional properties of $(K_{0.5}Na_{0.5})NbO_3$ piezoceramics by acceptor doping. J. Euro Ceram. Soc. **35**, 125–130 (2015)
25. F. Bortolani, A. del Campo, J.F. Fernandez, F. Clemens, F. Rubio-Marcos, High Strain in (K, Na)NbO_3–Based Lead-Free Piezoelectric Fibers. Chem. Mater. **12**, 3838–3848 (2014)
26. R. Bermejo, H. Gruenbichler, J. Kreith, C. Auer, Fracture resistance of a doped PZTceramic for multilayer piezoelectric actuators: effect of mechanical load and temperature. J. Eur. Ceram. Soc. **30**, 705–712 (2010)
27. J. Wang, X.-M. Chen, X.-M. Zhao, X.-X. Liang, X. Liu, P. Liu, Structure and dielectric property of Zr-doped $(Na_{0.47}Bi_{0.46}Ba_{0.06}K_{0.01})(Nb_{0.02}Ti_{0.98})O_3$ lead-free ceramics. J. Electroceram. **32**, 332–338 (2014)
28. R. Zuo, J. Fu, X. Wang, L. Li, Phase transition and domain variation contributions to piezoelectric properties of alkaline niobate based lead-free systems. J. Mater. Sci. **21**, 519–522 (2010)
29. Z. Zhang, R. Raj, Influence of grain size on ferroelastic toughening and piezoelectric behavior of lead zirconatetitanate. J. Am. Ceram. Soc. **78**, 3363–3368 (1995)
30. A. Garg, T.C. Goel, Mechanical and electrical properties of PZT ceramics (Zr:Ti = 0.40:0.60) related to Nd^{3+} addition. Mater. Sci. Eng. B **60**, 128–132 (1999)
31. A. Hizebry, M. Saadaoui, H. Elattaoui, J. Chevalier, G. Fantozzi, R-curve and subcritical crack growth in lead zirconatetitanate ceramics. Mater. Sci. Eng. A **499**, 368–373 (2009)
32. M. Promsawat, A. Watcharapasorn, S. Jiansirisomboon, Effects of ZnO nanoparticulate addition on the properties of PMNT ceramics. Nanoscale Res. Lett. **7**, 65–72 (2016)
33. A. Watcharapasorn, S. Jiansirisomboon, T. Tunkasiri, Microstructures and mechanical properties of zirconium-doped bismuth sodium titanate ceramics, Chiang Mai J. Sci., **33**, 169–173 (2006)